Total oxidation of methane over doped nanophase cerium oxides

A.E.C. Palmqvist [a,*,**], E.M. Johansson [b], S.G. Järås [b] and M. Muhammed [a,**]

[a] *Department of Materials Chemistry, Chemical Technology, Royal Institute of Technology (KTH), SE-100 44 Stockholm, Sweden*
[b] *Department of Chemical Engineering and Technology, Chemical Technology, Royal Institute of Technology (KTH), SE-100 44 Stockholm, Sweden*

Received 28 November 1997; accepted 1 October 1998

The formation of solid solutions of cerium oxide with the oxides of calcium, manganese, or neodymium enhances the catalytic activity of cerium oxide for the total oxidation of methane, whereas solid solutions with lead oxide showed an opposite effect. Reasons for this are discussed in terms of oxygen vacancy concentrations and mobilities, local structure configurations, number of oxidation states of dopant, and electron transfer properties. The effects of increased oxygen ion mobility and a more beneficial local structure support the increased catalytic activity for the calcium- and neodymium-doped cerium oxide samples. In addition, a reduced energy for charge transfer from oxygen to cerium supports a higher activity for the calcium-doped sample. The activity data were fitted to an Arrhenius equation, and the apparent activation energies were found to be between 110 and 130 kJ/mol. The particle sizes and the BET areas of the samples were only little affected by the reactor runs, and none of the samples were subjected to phase changes.

Keywords: catalyst preparation (doping), solid solution, oxalate coprecipitation, nanophase, ceria, oxygen vacancy, environmental, catalytic combustion, natural gas, oxygen ion mobility

1. Introduction

An interesting property of cerium oxide (CeO_2) is its ability to release and absorb oxygen during alternating redox conditions, and hence to function as oxygen buffer. As a part of car exhaust gas clean up catalysts, CeO_2 widens the "lambda window" in which the catalyst can simultaneously catalyze the reduction of NO and the oxidation of CO and hydrocarbons [1–3]. Efforts to increase the oxygen storage capacity of CeO_2 by the introduction of cation dopants have been successful [4]. Several samples of cerium-oxide-based solid solutions have been prepared with a variety of dopant cations, e.g., Ba, Ca, Co, Cu, Mn, Nd, Pb, Sr, Y, Zn, and Zr. Most of these materials showed enhancement of both oxygen vacancy concentration and oxygen storage capacity as well as of redox activities, compared to undoped CeO_2 [4]. The purpose of doping CeO_2 with dopants with a valence lower than 4+ is to create oxygen vacancies in the CeO_2 structure, in contrast to the more conventional doping of CeO_2 with ZrO_2 which is aimed to increase the thermal stability of CeO_2. The properties of the oxygen vacancies, e.g., local atomic structure and chemical environment, and binding energies, can in principle be controlled by the choice of dopants [5]. This is typical for nanostructured or nanophase catalytic materials.

Doping CeO_2 with Ca^{2+} ions has also been shown to increase the catalytic activity of CeO_2 for the reduction of SO_2 with CO [6]. The reasons for the higher catalytic activity of Ca-doped CeO_2 are discussed in a combined theoretical and experimental study [7]. The incorporation of Ca^{2+} ions in the CeO_2 structure leads to the formation of oxygen vacancies and to local structural changes where the coordinative unsaturation of specific Ce ions increases [8]. The computed energy for electron transfer from O^{2-} ions to Ce^{4+} ions has been found to be significantly reduced [7]. Preliminary results considering additional temperature-controlled distortions indicate that instantaneous geometrical structures exhibit even lower charge-transfer energies and a significant reactivity towards, e.g., hydrogen abstraction [9].

Metal oxide catalysts are also used in catalytic combustion applications, e.g., for fuel combustion [10] and in industrial abatement units for volatile organic compounds (VOC) [11]. Here, finding new metal oxide materials is desirable. The main advantage of metal oxide catalysts over noble metal catalysts are, in general, the lower cost of raw material, possible higher thermal stability and suppression of formation of nitrogen oxides from fuel-bound nitrogen [12,13]. Their main disadvantage is lower specific activity and the consequent higher ignition temperature [12]. The objective of the present work was to evaluate the conceptual ideas of oxygen vacancy formation through doping as a mean to increase the catalytic activity for methane oxidation over CeO_2. Methane was used for this study, since it is of great interest as a model compound for understanding the mechanisms of oxidation and catalytic combustion on metal oxides. It is also one of the least reactive hydrocarbons as well as being the main component in natural gas. Samples of doped CeO_2 were prepared, i.e., solid solutions were formed with CeO_2 and the oxide of an alkaline earth metal (Ca), a rare earth metal (Nd), a transition metal (Mn) and a group IVb metal (Pb). Oxygen vacancies were created through the formation of these solid solutions, and

* Formerly named A.E. Persson.
** To whom correspondence should be addressed.

their catalytic activities were compared to that of an undoped CeO_2 sample.

2. Experimental

2.1. Chemicals, solutions, and synthesis

The synthesis of the doped CeO_2 samples has been presented in detail in previous papers [5,6] and will here only be briefly described. Suitable synthesis conditions were obtained via computer modeling using the CEC software [14]. 1.0 or 2.0 M solutions of the dopant nitrates were mixed at the desired molar ratios with a cerium nitrate solution. The mixed solution was then added drop-wise to a 0.2 M ammonium oxalate solution at a suitable pH at which oxalate coprecipitates formed. The precipitate was washed with water and then dried at 80 °C for a few days after which it was calcined for 4.5 h at 600 °C in air in a muffle furnace to produce the oxide solid solutions.

2.2. Powder characterization

The methods of characterization used in this study have been thoroughly described earlier [6] and will only shortly be presented here. Chemical composition of the products was determined with an ARL 3520B inductively coupled plasma atomic emission spectrophotometer (ICP-AES). The oxygen deficiency value (δ) in $Ce_{1-x}M_xO_{2-\delta}$ was determined at room temperature by a redox titrimetric method. Crystal phase analysis was performed with a Rigaku CN2182D6 theta–theta X-ray diffractometer (XRD) using Cu K_α radiation. The average particle sizes were calculated applying the Scherrer equation [15] to the XRD line broadening. Unit cell parameters were obtained through Guinier camera XRD measurements using powdered aluminum as an internal standard. Specific surface areas were measured by N_2 adsorption according to the 5-point BET method with a Micromeritics Gemini 2370 instrument at −196 °C.

2.3. Catalytic evaluation

Catalytic activity of the samples was studied with a packed-bed quartz microreactor, with an inner diameter of 6 mm, vertically mounted in a tubular furnace. The temperature was measured with a thermocouple directly on top of the catalyst powder. The samples were pre-treated *in situ* in air at 600 °C for 10 min, to obtain similar starting conditions for the different samples, after which they were cooled down to 250 °C. The samples were then exposed to a gas mixture containing 1.4% CH_4 and 25% O_2 in He, and the temperature was increased at a rate of 5 °C/min to 600 °C at which it was held for 10 min. The samples were subsequently cooled by 5 °C/min while exposed to the gas mixture. During the runs, the outlet gases were analyzed with a Balzers mass spectrometer model QMG421C. After the first reactor run, some of the samples, namely the Nd31, Mn2, and Ce100, were left in the reactor and subject to a second reactor run. The second run was carried out in the same way as the first, except that there was no additional pre-treatment in air, and that the gas composition was 1.4% CH_4 and 6% O_2 in He. In all runs, 0.3 g of sample powder and a space velocity of 40 000 ml(gas)/h g(catalyst) were used. The samples were finally analyzed with XRD to check for phase changes.

3. Results

3.1. Sample characterization

Chemical compositions of the studied samples are given in table 1. XRD patterns of the samples revealed that the powders consisted of solid solutions of $Ce_{1-x}M_xO_{2-\delta}$, as shown in figure 1(a). The doped samples retain the fluorite structure of pure CeO_2, with slightly distorted lattices as shown by their unit cell parameters given in table 1. The oxygen deficiency values (δ) show the presence of oxygen vacancies at room temperature in air, in all samples, except from the Ce100 and Mn2. Some values are remarkably close to those expected when considering the most likely values of the dopant oxidation state. The average particle sizes of the samples after calcination are small (15–20 nm) and the specific surface areas in the range of 29–43 m^2/g.

3.2. Catalytic evaluation

Figure 2 shows the fraction of methane that has been converted to CO_2 and H_2O over the different cerium oxide samples studied versus the inlet gas temperature. A complete oxidation of methane is achieved and the typical products of an incomplete oxidation, e.g., CO and H_2, were not detected for any of the samples studied. A considerable difference in catalytic activity for the different samples is observed, where the Nd11 sample showed the highest activity followed, in order of decreasing activity, by the Mn2, Nd31, Ca10, Ce100, and with much lower activity the Pb11 sample. The temperatures, T_{20} and T_{50}, corresponding to 20 and 50% conversion of methane, respectively, are given

Table 1
Characteristics of the cerium oxide samples studied.

Sample	Composition	δ[a]	a[b] (Å)	d_1[c] (nm)	S_1[d] (m^2/g)
Ce100	$CeO_{2-\delta}$	0.00	5.412	20.9	29.5
Ca10	$Ce_{0.90}Ca_{0.10}O_{2-\delta}$	0.09	5.416	17.8	29.3
Mn2	$Ce_{0.98}Mn_{0.02}O_{2-\delta}$	−0.02	5.418	15.9	42.6
Pb11	$Ce_{0.89}Pb_{0.11}O_{2-\delta}$	0.16	5.419	13.8	35.7
Nd11	$Ce_{0.89}Nd_{0.11}O_{2-\delta}$	0.06	5.432	15.5	33.8
Nd31	$Ce_{0.69}Nd_{0.31}O_{2-\delta}$	0.18	5.461	11.7[e]	30.7

[a] δ is the oxygen deficiency in the composition $Ce_{1-x}M_xO_{2-\delta}$.
[b] a is the unit cell parameter.
[c] d_1 is the average particle size determined by XRD line broadening.
[d] S_1 is the BET area of the fresh samples.
[e] Sample composition differs much from composition of standard sample (CeO_2). This makes the calculated value slightly lower than the "real" value.

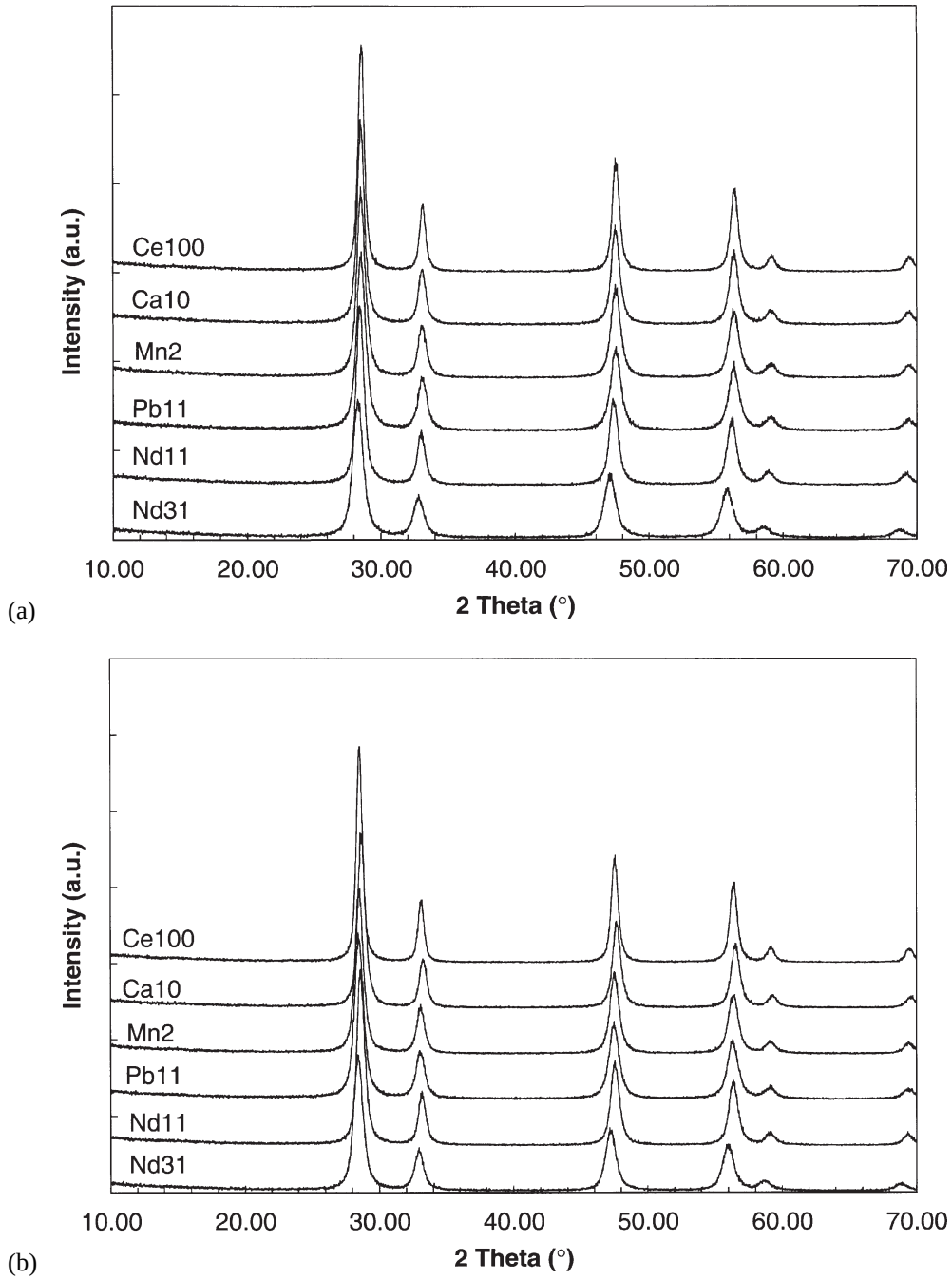

Figure 1. X-ray diffractograms of the samples listed in table 1: before (a) and after (b) the catalytic activity evaluation.

in table 2. The reproducibility of the reactor runs was investigated by performing two independent runs on two different Ce100 samples. The T_{20} and T_{50} temperatures of the two runs were found to agree within 5 °C, which may be compared to the largest difference between two samples, i.e., 84 °C. No phase change was observed by XRD of the samples after the reactor studies, as shown in figure 1(b). Relatively small changes (<10%) were observed on the BET areas for all samples except for the Nd31 and Pb11 samples as a result of the reactor runs. The changes in particle size were also small (<4%), except for the Nd31 sample (table 2).

The reaction rate equation for total oxidation of methane is in reality very complex, involving the competition of sites, and several coupled temperature dependent adsorption equilibria of molecules such as CO, CO_2, and H_2O, besides CH_4 and O_2. However, a reasonably good agreement is generally obtained for the reaction rate of total oxidation of methane using the simplified semi-empirical equation [12,16,17]:

$$r = \left(k'_{\mathrm{s}}(T)p_{\mathrm{O_2}}^{1/2} + k'_{1}(T)\right)p_{\mathrm{CH_4}}, \tag{1}$$

where the overall rate constant of surface chemisorbed oxygen is represented by $k'_{\mathrm{s}}(T)$ and the overall rate constant

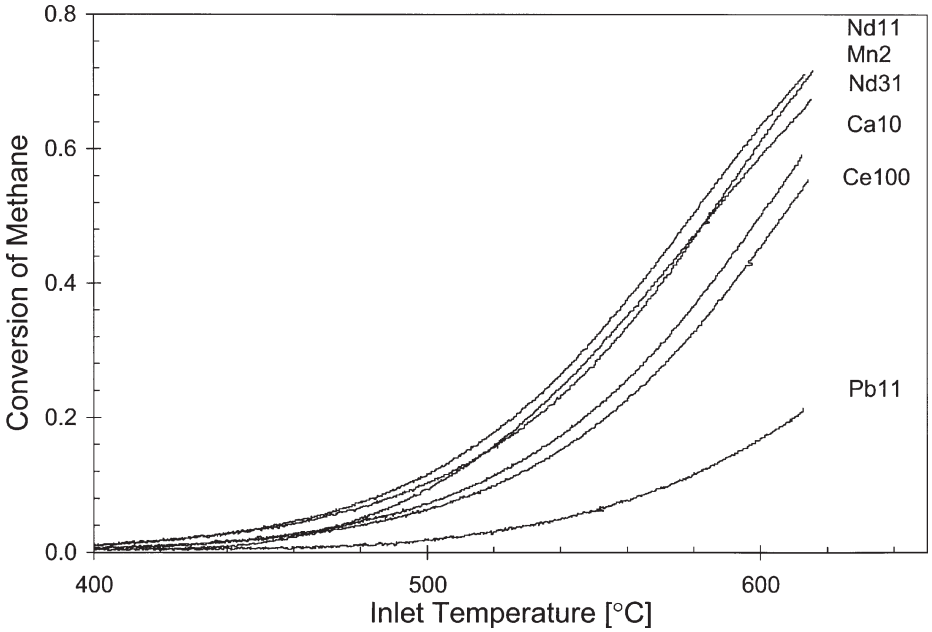

Figure 2. Fraction of methane converted to CO_2 and H_2O versus the inlet gas temperature for samples Ce100, Ca10, Mn2, Pb11, Nd11, and Nd31. $p_{CH_4} = 1.4\%$, $p_{O_2} = 25\%$, temperature increase rate $= 5\,^{\circ}$C/min, space velocity $= 40\,000$ ml(gas)/h g(catalyst). Actual raw data is displayed.

Table 2
Catalytic performance of the cerium oxide samples studied.

Sample	T_{20}[a] (°C)	T_{50}[a] (°C)	S_2[b] (m^2/g)	d_2[c] (nm)	E_a[d] (kJ/mol)	ln A[e]
Ce100	553	607	27.6	21.8	112	14.0
Ca10	547	600	26.3	17.8	122	15.7
Mn2	530	585	41.3[f]	15.5	116	15.2
Pb11	609	–	29.3	13.9	127	15.2
Nd11	525	579	33.8	16.0	116	15.4
Nd31	532	585	24.5[f]	13.9[g]	–	–

[a] T_{20} and T_{50} are the temperatures corresponding to 20 and 50% conversion, respectively.
[b] S_2 is the BET surface area of samples after CH_4 oxidation.
[c] d_2 is the average particle size after CH_4 oxidation.
[d] E_a is the apparent activation energy calculated from the temperature dependence of the catalytic activity measurements.
[e] ln A is the logarithm of the pre-exponential factor for the CH_4 oxidation.
[f] BET area after two consecutive CH_4 oxidation runs.
[g] Sample composition differs much from composition of standard sample (CeO_2). This makes the calculated value slightly lower than the "real" value.

of lattice oxygen by $k_1'(T)$. The partial pressures of oxygen and methane are denoted p_{O_2} and p_{CH_2}, respectively. Equation (1) can be further simplified assuming prevailing conditions of a fast supply of oxygen from the gas phase to substitute the consumed lattice oxygen, and negligible inhibiting effects of CO_2 and H_2O (dry gases, low concentration of CH_4, temperatures above 400 °C, and converted fractions below 0.7). Under these conditions, the reaction rate of oxidation of methane can thus be expressed as

$$r = k'' p_{CH_4}, \tag{2}$$

where k'' is the overall effective rate constant for the reaction. Figure 3 shows the Arrhenius plots of the natural logarithm of the rate constants versus the reciprocal temperature, where k'' is fitted to the equation

$$k'' = A \exp\left(-\frac{E_a}{RT}\right). \tag{3}$$

As seen, all samples with the exception of the Nd31 sample, gave a linear dependency. Sample Nd31 did, however, show a linear dependence in the subsequent study where an oxygen concentration of 6% was used. The reason for this is discussed in section 3.3. The values of the natural logarithm of the overall pre-exponential factor, ln A, and the apparent activation energy, E_a, could be extracted from the intercept and slope, respectively, of the curves in figure 3, and are presented in table 2. The values of ln A and E_a correspond to the overall rate constants for the samples. The overall apparent activation energies of the samples range from 110–130 kJ/mol, which falls in the range expected for these moderately active metal oxides [16–18]. The values of the pre-exponential factor is 3–6 times higher for the doped samples compared to the undoped.

3.3. Effects of oxygen partial pressure on the oxidation of CH_4

In figure 4, the fraction of methane that has been converted to CO_2 and H_2O over the three samples Ce100, Mn2, and Nd31 at two different oxygen partial pressures is plotted versus temperature. This shows that the change in T_{50} value due to a lowering of oxygen partial pressure is much larger for the Ce100 and Mn2 samples than for the Nd31 sample. Figure 5 shows the natural logarithm of the rate constants versus the reciprocal of the temperature for the three samples at the two different oxygen partial pressures studied. The non-linear shape of the Nd31 sample, found

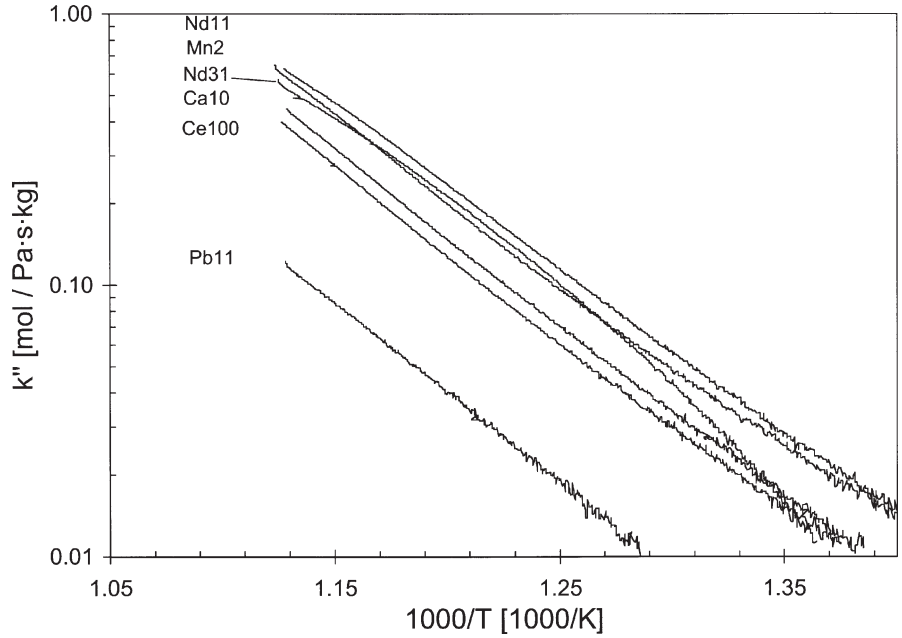

Figure 3. The overall rate constants, k'', of the studied samples as a function of the reciprocal of the temperature. $p_{CH_4} = 1.4\%$, $p_{O_2} = 25\%$, temperature increase rate = 5 °C/min, space velocity = 40 000 ml(gas)/h g(catalyst).

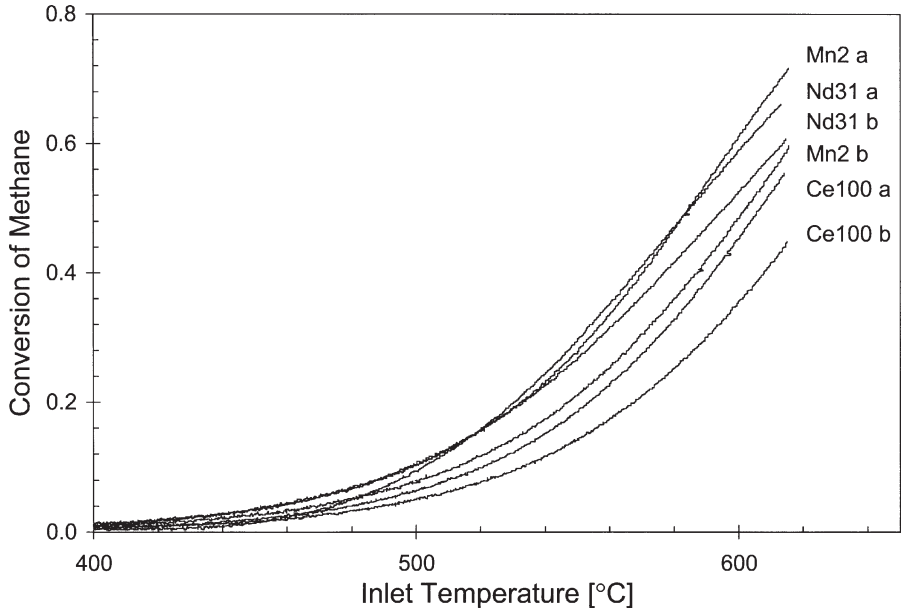

Figure 4. Fraction of methane converted to CO_2 and H_2O versus the inlet gas temperature for samples Ce100, Mn2, and Nd31 at two different oxygen partial pressures: $p_{O_2} = 25\%$ (a) and $p_{O_2} = 6\%$ (b). $p_{CH_4} = 1.4\%$, temperature increase rate = 5 °C/min, space velocity = 40 000 ml(gas)/h g(catalyst).

for the run with 25% O_2 concentration, was not found as the same sample was subsequently exposed to the 6% O_2 run. This is interpreted as an *in situ* activation of the Nd31 sample during the exposure to the CH_4/O_2 gas mixture in the first run.

4. Discussion

The reactivity of metal oxides is largely dependent on the degree of the coordinative unsaturation of metal ions it exhibits. Especially the presence of oxygen vacancies efficiently exposes highly unsaturated cations [19,20]. For cerium oxide, the cerium ion may have two oxidation states, which allows it to participate in reactions that involve changes in the oxidation state of the cation. Due to the coordinative unsaturation at the surface underlying lattice oxygen ions are, generally, weaker bound than those of the bulk. This allows these underlying oxygens to participate in oxidation reactions [19]. By substituting part of the Ce^{4+} in the CeO_2 structure by other cations, the coordina-

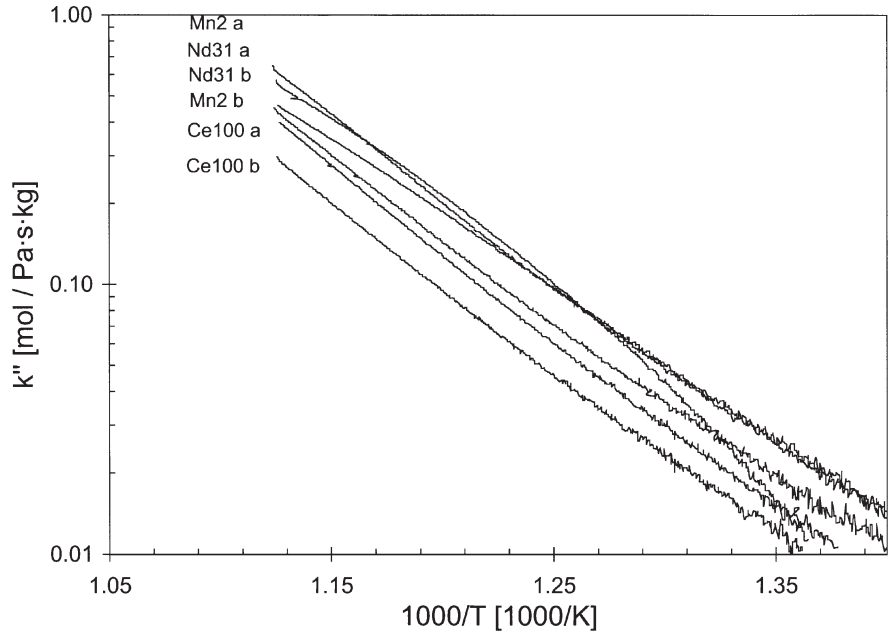

Figure 5. The overall rate constants, k'', of the Ce100, Mn2, and Nd31 samples as a function of the reciprocal of the temperature at two different oxygen partial pressures: $p_{O_2} = 25\%$ (a) and $p_{O_2} = 6\%$ (b). $p_{CH_4} = 1.4\%$, temperature increase rate = 5 °C/min, space velocity = 40 000 ml(gas)/h g(catalyst).

tive unsaturation of the cerium ions is increased. There are other factors, possibly affecting the catalytic activity, that are also altered by the introduction of dopants, e.g., oxygen vacancy mobility, acid/base properties, local structure, and electron affinities of cerium ions [7,8,21–25].

For the total oxidation of CH_4 over a metal oxide catalyst, some elementary steps will involve the transport of oxygen ions from the catalyst to the products of CO_2 and H_2O. In the case that such a step is rate determining, the mobility of the oxygen ions can be expected to influence the overall catalytic activity of the material. Doping CeO_2 with cations with a valence state lower than 4+ introduces oxygen vacancies in the crystal structure. These oxygen vacancies are expected to be active sites for the oxygen transfer in the catalytic oxidation of methane. As such, their concentration and mobility in the lattice and surface of the material should influence the overall catalytic activity. Nd- and Ca-doped CeO_2 samples have shown higher ionic conductivities than the undoped CeO_2 [21–24], and so the currently presented results indicate a possible correlation between the oxygen ion mobility and the catalytic activity for methane oxidation over these samples. No oxygen ion mobility data for Pb- and Mn-doped CeO_2 samples were found in the literature.

In addition to the oxygen transfer processes, other elementary steps of the oxidation of methane involve charge transfer processes. Although the mechanism of the oxidation of methane over metal oxide catalysts is not fully understood, it is expected that electrons are transferred from the methane molecule to the oxygen molecule via the catalyst surface [20]. If an elementary step involving an electron transfer process is rate determining, the charge transfer energy and the electron affinity of the cerium and the dopant ions would be expected to determine the overall catalytic activity of the material. In fact, quantum chemical calculations have shown that the electron affinity of the Ce^{4+} ion decreases at certain surface sites and increases at others for a Ca-doped CeO_2(110) surface as compared to Ce^{4+} ions in an undoped CeO_2(110) surface [7]. Even more interestingly, the energy for charge transfer from oxygen ions to cerium ions was shown to be lowered for the Ca-doped surface as compared to the undoped surface [7]. Some of the dopants in the present study (Pb and Mn) have several different oxidation states, whereas others (Ca and Nd) have only a single oxidation state. For this reason, the Pb and Mn dopants are expected to have a larger influence on the charge transfer processes themselves (by changing oxidation state) as compared to the Ca and Nd dopants. The Ca and Nd dopants have, however, the indirect effect on charge transfer reactions due to their influence on local structure and the effect this has on charge transfer energy [7,8].

The abstraction of hydrogen from the CH_4 molecule is generally thought of as the first step in the oxidation of methane, and the acid/base character of the catalyst affects how readily this step occurs. Preliminary quantum chemical calculations have shown an increased reactivity for hydrogen abstraction upon Ca-doping of CeO_2 [9]. Earlier work at our laboratory [4] has shown Pb-doped CeO_2 to be much more readily reduced with H_2 than the other samples studied in the present work. This supports the explanation that the low catalytic activity of the Pb-doped sample is related to either low oxygen ion mobility or low tendency for the release of electrons to oxygen molecules. Pb-doped CeO_2 has a different local structure than the other samples [8]. This may also be the cause of the lower catalytic activity observed for the system. On the other hand, the

deactivation of catalysts by Pb, such as deposition of lead compounds from automotive fuels on exhaust gas catalysts, is of course well-known from earlier studies [26]. Pb in the form of deposited compounds is in a chemically different form compared to that in the Pb-doped catalysts studied in the present work, and the low catalytic activity found for the Pb-doped CeO_2 is hence not explained by the current knowledge of Pb-poisoning regarding automotive catalysts.

5. Conclusion

Catalytic activities for the oxidation of methane were found to increase as a result of doping CeO_2 with Ca, Mn, and Nd cations. However, Pb-doped CeO_2 was found to have much lower activity than the undoped CeO_2. Doping CeO_2 with cations of lower valence than $4+$ introduces defects, oxygen vacancies, in the fluorite crystal structure as solid solutions are formed. This process generates active sites for the reaction and, besides the increased concentration and mobility of vacancies, the energy for charge transfer from oxygen to cerium is lowered (at least in the case with Ca-doping). These effects should be beneficial for the catalytic activity of the materials. The reasons for the lower activity found for the Pb-doped CeO_2 is currently not fully understood.

Acknowledgement

Financial support from the Materials Consortium of Clusters and Ultrafine Particles, and the Swedish Research Council for Engineering Sciences (TFR) is greatly acknowledged. Thanks are also due to Professor P.G. Menon for valuable discussions and comments.

References

[1] T. Kreuzer, E.S. Lox, D. Lindner and J. Leyrer, Catal. Today 29 (1996) 17.
[2] K.C. Taylor, in: *Catalysis Science and Technology*, Vol. 5, eds. M. Boudart and J.R. Anderson (Springer, Berlin, 1984) p. 120.
[3] R.M. Heck and R.J. Farrauto, *Catalytic Air Pollution Control – Commercial Technology* (Van Nostrand, New York, 1995).
[4] Y. Zhang, S. Andersson and M. Muhammed, Appl. Catal. B 6 (1995) 325.
[5] A.E. Persson, Y. Zhang and M. Muhammed, in: *Catalyst Materials for High Temperature Processes, Ceramic Transactions*, Vol. 73, eds. K.S. Ramesh, M. Misono and P.L. Gai (Am. Ceram. Soc., Westerville, OH, 1997) p. 85.
[6] A.E.C. Palmqvist, M.F.M. Zwinkels, Y. Zhang, S.G. Järås and M. Muhammed, Nanostruct. Mater. 8 (1997) 801.
[7] S. de Carolis, J.-L. Pascual, L.G.M. Pettersson, M. Baudin, M. Wójcik, K. Hermansson, A.E.C. Palmqvist and M. Muhammed, J. Phys. Chem., submitted.
[8] A.E.C. Palmqvist, P. Berastegui, S. Eriksson, A. Hannon, L. Furenlid, M. Baudin, M. Wójcik and K. Hermansson, to be published.
[9] S. de Carolis, J.-L. Pascual, L.G.M. Pettersson, M. Baudin, M. Wójcik, K. Hermansson and A.E.C. Palmqvist, to be published.
[10] R.E. Hayes and S.T. Kolaczkowski, *Introduction to Catalytic Combustion* (Gordon and Breach, Amsterdam, 1997).
[11] J.J. Spivey, in: *Catalysis – Specialist Periodical Report*, Vol. 8 (Roy. Soc. Chem., 1989) p. 157.
[12] M.F.M. Zwinkels, S.G. Järås, P.G. Menon and T.A. Griffin, Catal. Rev. Sci. Eng. 35 (1993) 319.
[13] E.M. Johansson and S.G. Järås, in: *3rd International Workshop on Catalytic Combustion*, Amsterdam, The Netherlands, 23–25 September 1996, in press.
[14] M. Wang and M. Muhammed, CEC (Software for modeling of chemical solution equilibria), to be published.
[15] H.P. Klug and L.E. Alexander, *X-Ray Diffraction Procedures*, 2nd Ed. (Wiley, New York, 1974).
[16] E.M. Johansson, J.G. McCarty and S.G. Järås, Appl. Catal. A, submitted.
[17] H. Arai, T. Yamada, K. Eguchi and T. Seiyama, Appl. Catal. 26 (1986) 265.
[18] M.A. Quinlan, H. Wise and J.G. McCarty, GRI Report 89/0141 (1989).
[19] R.A. van Santen and J.W. Niemantsverdriet, *Chemical Kinetics and Catalysis* (Plenum Press, New York, 1995).
[20] H. Wise and J. Oudar, *Materials Concepts in Surface Reactivity and Catalysis* (Academic Press, San Diego, 1990).
[21] T. Kudo and H. Obayashi, J. Electrochem. Soc. 122 (1975) 142.
[22] R.T. Dirstine, R.N. Blumenthal and T.F. Kuech, J. Electrochem. Soc. 126 (1979) 264.
[23] H. Yashiro, T. Ohuchi, K. Eguchi and H. Arai, J. Mater. Sci. 23 (1988) 1036.
[24] H. Inaba and H. Tagawa, Yokohama Kokuritsu Daigaku Kankyo Kagaku Kenkyu Senta Kiyo 21 (1995) 203.
[25] W. Liu and M. Flytzani-Stephanopoulos, J. Catal. 153 (1995) 304.
[26] M. Shelef, K. Otto and N.C. Otto, Adv. Catal. 27 (1978) 311.